Measuring coherence functions using non-parallel double slits

Shawn Divitt,* Zachary J. Lapin, and Lukas Novotny

ETH Zürich, Photonics Laboratory, 8093 Zürich, Switzerland

*sdivitt@ethz.ch

Abstract: We present an experimental method for the fast measurement of both the spectral (spatial) and complex degrees of coherence of an optical field using only a binary amplitude mask and a detector array. We test the method by measuring a two-dimensional spectral degree of coherence function created by a broadband thermal source. The results are compared to those expected by the van Cittert-Zernike theorem and found to agree well in both amplitude and phase.

OCIS codes: (030.0030) Coherence and statistical optics; (050.1220) Apertures; (050.1940) Diffraction; (120.0120) Instrumentation, measurement, and metrology.

References and links

1. B. J. Thompson and E. Wolf, "Two-beam interference with partially coherent light," J. Opt. Soc. Am. **47**, 895–902 (1957).
2. E. Tervonen, J. Turunen, and A. Friberg, "Transverse laser-mode structure determination from spatial coherence measurements: Experimental results," Appl. Phys. B **49**, 409–414 (1989).
3. D. Ambrosini, G. S. Spagnolo, D. Paoletti, and S. Vicalvi, "High-precision digital automated measurement of degree of coherence in the Thompson and Wolf experiment," Pure Appl. Opt. **7**, 933–939 (1998).
4. C. Iaconis and I. A. Walmsley, "Direct measurement of the two-point field correlation function," Opt. Lett. **21**, 1783–1785 (1996).
5. S. Titus, A. Wasan, J. Vaishya, and H. Kandpal, "Determination of phase and amplitude of degree of coherence from spectroscopic measurements," Opt. Commun. **173**, 45–49 (2000).
6. H. Kandpal and J. Vaishya, "Experimental study of coherence properties of light fields in the region of superposition in Young's interference experiment," Opt. Commun. **186**, 15–20 (2000).
7. L. Basano, P. Ottonello, G. Rottigni, and M. Vicari, "Degree of spectral coherence, space-frequency plots and correlation-induced spectral changes," Opt. Commun. **207**, 77–83 (2002).
8. L. Basano, P. Ottonello, G. Rottigni, and M. Vicari, "Spatial and temporal coherence of filtered thermal light," Appl. Opt. **42**, 6239–6244 (2003).
9. J. J. A. Lin, D. Paterson, A. G. Peele, P. J. McMahon, C. T. Chantler, K. A. Nugent, B. Lai, N. Moldovan, Z. Cai, D. C. Mancini, and I. McNulty, "Measurement of the spatial coherence function of undulator radiation using a phase mask," Phys. Rev. Lett. **90**, 074801 (2003).
10. P. Petruck, R. Riesenberg, U. Hübner, and R. Kowarschik, "Spatial coherence on micrometer scale measured by a nanohole array," Opt. Commun. **285**, 389–392 (2012).
11. Y. Mejía and A. I. González, "Measuring spatial coherence by using a mask with multiple apertures," Opt. Commun. **273**, 428–434 (2007).
12. A. I. González and Y. Mejía, "Nonredundant array of apertures to measure the spatial coherence in two dimensions with only one interferogram," J. Opt. Soc. Am. A **28**, 1107–1113 (2011).
13. D. F. Siriani, "Beyond Young's experiment: time-domain correlation measurement in a pinhole array," Opt. Lett. **38**, 857–859 (2013).
14. M. Santarsiero and R. Borghi, "Measuring spatial coherence by using a reversed-wavefront Young interferometer," Opt. Lett. **31**, 861–863 (2006).
15. J.-M. Choi, "Measuring optical spatial coherence by using a programmable aperture," J. Korean Phys. Soc. **60**, 177–180 (2012).
16. K. Saastamoinen, J. Tervo, J. Turunen, P. Vahimaa, and A. T. Friberg, "Spatial coherence measurement of polychromatic light with modified Young's interferometer," Opt. Express **21**, 4061–4071 (2013).

#204319 - $15.00 USD Received 10 Jan 2014; revised 20 Mar 2014; accepted 22 Mar 2014; published 1 Apr 2014

17. A. Cámara, J. A. Rodrigo, and T. Alieva, "Optical coherenscopy based on phase-space tomography," Opt. Express **21**, 13169–13183 (2013).
18. L. Waller, G. Situ, and J. W. Fleischer, "Phase-space measurement and coherence synthesis of optical beams," Nat. Photonics **6**, 474–479 (2012).
19. S. Cho, M. A. Alonso, and T. G. Brown, "Measurement of spatial coherence through diffraction from a transparent mask with a phase discontinuity," Opt. Lett. **37**, 2724–2726 (2012).
20. M. A. Alonso, "Wigner functions in optics: describing beams as ray bundles and pulses as particle ensembles," Adv. Opt. Photonics **3**, 272–365 (2011).
21. E. Mukamel, K. Banaszek, I. A. Walmsley, and C. Dorrer, "Direct measurement of the spatial Wigner function with area-integrated detection," Opt. Lett. **28**, 1317–1319 (2003).
22. D. F. McAlister, M. Beck, L. Clarke, A. Mayer, and M. G. Raymer, "Optical phase retrieval by phase-space tomography and fractional-order Fourier transforms," Opt. Lett. **20**, 1181–1183 (1995).
23. T. Young, "On the nature of light and colours," in *A Course of Lectures on Natural Philosophy and the Mechanical Arts* (J. Johnson, 1807), Vol. 1, pp. 464–465.
24. E. Wolf, *Introduction to the Theory of Coherence and Polarization of Light* (Cambridge University, 2007).
25. J. Goodman, *Introduction to Fourier Optics* (Roberts, 2005).
26. R. A. Bartels, A. Paul, M. M. Murnane, H. C. Kapteyn, S. Backus, Y. Liu, and D. T. Attwood, "Absolute determination of the wavelength and spectrum of an extreme-ultraviolet beam by a Young's double-slit measurement," Opt. Lett. **27**, 707–709 (2002).
27. A. T. Friberg and E. Wolf, "Relationships between the complex degrees of coherence in the space–time and in the space–frequency domains," Opt. Lett. **20**, 623–625 (1995).
28. E. Wolf, "Young's interference fringes with narrow-band light," Opt. Lett. **8**, 250–252 (1983).

1. Introduction

Many general methodologies for measuring the second-order coherence properties of a light field have been developed since the pioneering experiments of Thompson and Wolf [1]. In particular, the complex degree of coherence can be measured through a series of Thompson-Wolf experiments or other interferometric methods [2–16]. The same coherence function can also be extracted through measurements of related functions which represent transformations of the mutual coherence function over one or more of its variables, such as Wigner or ambiguity functions [17–22]. Among the various methods, trade-offs are made between experiment time and complexity, post-processing requirements, and restrictions to fields with specific properties such as limited spectral bandwidth or Schell-model behavior.

Interferometric methods are of interest because they been extensively studied and offer relatively direct measurements of coherence. Within the interferometric methods, several clever solutions stand out. These solutions include automated methods for controlling the placement of two pinholes [2, 3], Sagnac interferometry [4], spectroscopic or optically filtered measurements [5–8], redundant [9, 10] and non-redundant [11–13] arrays of pinholes or slits, reversed-wavefront interferometry [14], programmable apertures [15], and diffractive elements which modify a two-pinhole interference pattern [16].

In this paper we present a method and an apparatus inspired by the experiments of Young [23] and Thompson and Wolf which allow for measurement of the amplitude and phase of both spectral and complex degrees of coherence in a simple and robust fashion. A diagram of the apparatus is given in Fig. 1. The method makes use of a two-slit aperture in which the slit-to-slit separation varies slowly along one dimension (cf. Fig. 2). The interferogram generated by the aperture is used to approximate an ensemble of simultaneous Thompson-Wolf experiments.

The method stands apart from others by offering the capability of measuring field correlations created by a broadband source over a wide range of pinhole separations using only a binary amplitude mask and a detector array. While non-redundant pinhole arrays have been shown via numerical modeling to have similar capabilities [13], they have not been shown to be applicable to arbitrarily broadband fields. In terms of spectral bandwidth limitations, the method considered in this paper is limited mainly by the spectral response function of the detector, which is a general constraint of all optical experiments. In order to demonstrate the method, we present a

#204319 - $15.00 USD Received 10 Jan 2014; revised 20 Mar 2014; accepted 22 Mar 2014; published 1 Apr 2014

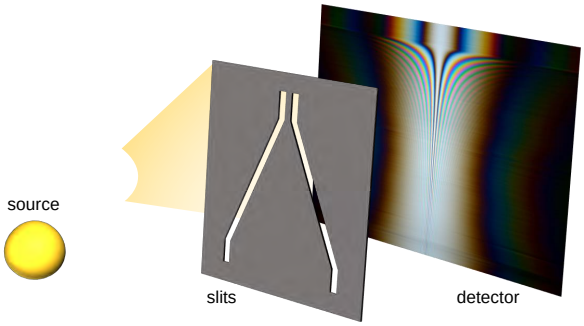

Fig. 1. A diagram (not drawn to scale) of the essential elements of the apparatus. Broadband light from an extended source passes through the non-parallel double slit aperture and generates an interference pattern on the detector plane.

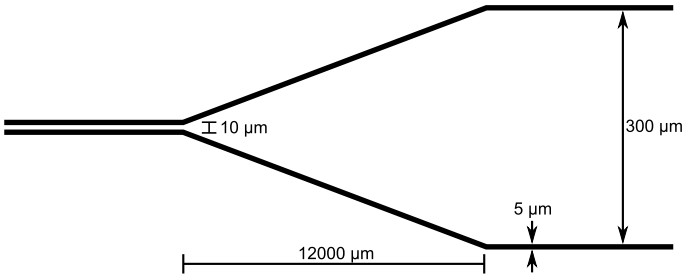

Fig. 2. A schematic (not drawn to scale) of the two-slit aperture used to measure coherence functions. The black lines represent transparent slits and white represents areas of high opacity.

measurement of the spectral degree of coherence of light emitted by a thermal source emitting across the visible wavelength range and compare the results to those which are expected by the van Cittert-Zernike theorem [24].

2. Apparatus design and calibration

An aperture was designed that could be used to approximate an ensemble of simultaneous Thompson-Wolf experiments. The aperture contains a pair of slits as shown in Fig. 2. The slits have three characteristic dimensions, namely the slit length, width, and the slit-to-slit separation. These dimensions govern the diffraction effects that are expected from such an aperture. The aperture is fastened onto the lens mount of a digital camera, replacing the lens. This is done using a 1 inch (1 in. = 2.54 cm) diameter lens tube and a mounting adapter. This constitutes the entire apparatus and offers a high degree of stability and portability.

The specific dimensions of the aperture were chosen in order to measure the correlations of optical fields from sources with an appreciable apparent size without requiring any additional optics. The aperture consists of two parallel regions and one non-parallel region. The non-parallel region allows for measurement of the coherence functions; the slow variation in slit-to-slit separation enables a two-dimensional interference pattern to be recorded in which certain cross-sections represent Thompson-Wolf experiments. The parallel regions serve two purposes. First, they reduce the effect of ringing, or knife-edge diffraction, that would otherwise occur at

#204319 - $15.00 USD Received 10 Jan 2014; revised 20 Mar 2014; accepted 22 Mar 2014; published 1 Apr 2014

the top and bottom edges of the non-parallel region. Second, they allow for calibration of the aperture-to-detector distance and for aperture/detector rotational alignment.

Rotational alignment of the aperture to the detector and measurement of the aperture-to-detector distance were both accomplished by examining interferograms created under illumination by a laser. Certain symmetric positions in the interferogram were used as reference positions. The aperture was rotated by hand until the difference in the vertical position of these two points was less than 20 pixels as measured on the detector, corresponding to an angular error of ± 0.4 degrees. The distance measurement was accomplished by fitting the interferogram with the first Rayleigh-Sommerfeld diffraction solution under the scalar field approximation [25]. A cross-section of the interferogram corresponding to the parallel, 300 μm slit-to-slit separation region was used in the fitting because of the well known separation distance and high fringe-frequency which provided the highest precision. The measurement found an aperture-to-detector distance of 6.19 cm and was precise enough to detect distance changes on the order of 100 μm.

3. Theoretical foundations

Given that a Thompson-Wolf experiment is being performed, we can extract the coherence functions from the generated interference pattern. We begin by considering the intensity distribution at an observation plane that is behind, parallel to, and sufficiently distant from a two-pinhole aperture plane. A diagram of this situation is given in Fig. 3. We assume that both pinholes are the same size and are illuminated with the same power spectral density and that we have stationary and ergodic optical fields. We also consider all power spectra to be given in the analytic signal representation.

In general, we are interested in measuring the complex degree of coherence, $\gamma_\tau(\tau)$, and the spectral degree of coherence, $\mu_\omega(\omega)$, of the light at the two pinholes. Here, τ represents the time difference between measurements of the light field at one pinhole vs. the other and ω is the angular frequency of a particular quasi-monochromatic component of the field. Neither of the fundamental parameters τ or ω is directly accessible under experimental conditions. Rather, the accessible parameters are position and, through a Fourier transform, spatial frequency. The accessible parameters happen to be related to the fundamental ones as a consequence of diffraction.

Under the far-field approximation, the position coordinate x is related to τ by $x = zc\tau/d$, where c is the speed of light in air, z is the distance between the aperture and the detector along the z'-axis, and d is the pinhole center-to-center separation. Similarly, the spatial frequency coordinate f_x is related to ω under the far-field approximation by $\omega = 2\pi zcf_x/d$. The functions associated with the accessible parameters, $\gamma(x)$ and $\mu(f_x)$, can ultimately be transformed into $\gamma_\tau(\tau)$ and $\mu_\omega(\omega)$ using the aforementioned relations. Explicitly, $\gamma_\tau(\tau) = \gamma_\tau(dx/[zc]) = \gamma(zc\tau/d) = \gamma(x)$ and $\mu_\omega(\omega) = \mu_\omega(2\pi zcf_x/d) = \mu(\omega d/[2\pi zc]) = \mu(f_x)$.

3.1. The spatial intensity distribution

We now consider the power spectral density of light along the x-axis in Fig. 3, which we define as $S(x,\omega)$. The intensity along the x-axis, which is the measurable quantity of interest, is given by $I(x) = \int_{-\infty}^{\infty} S(x,\omega)\,\mathrm{d}\omega$. Following the formulas regarding $S(x,\omega)$ given by Wolf [24] in Sec. 4.2, we find the intensity distribution can be rewritten as

$$I(x) = \int_{-\infty}^{\infty} 2|K(x,\omega)|^2 S_Q(\omega)\left(1 + \mathrm{Re}\left[\mu_\omega(\omega)\exp\left(-i\frac{\omega x d}{zc}\right)\right]\right)\mathrm{d}\omega, \tag{1}$$

where x is the spatial coordinate as given along the x-axis in Fig. 3, $K(x,\omega)$ is separable such that $K(x,\omega) = K_x(x)K_\omega(\omega)$ and is related to single-pinhole diffraction effects, and $S_Q(\omega)$ is

#204319 - $15.00 USD Received 10 Jan 2014; revised 20 Mar 2014; accepted 22 Mar 2014; published 1 Apr 2014

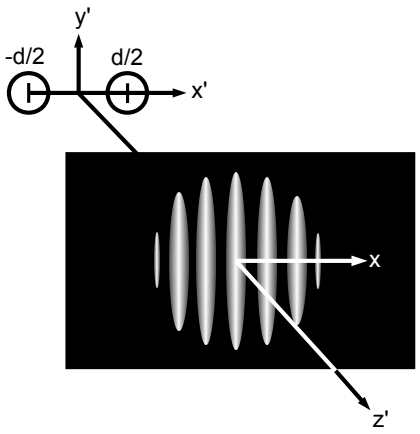

Fig. 3. A diagram (not drawn to scale) of a Thompson-Wolf experiment as given in the Cartesian coordinates used in the text. The two circles represent pinholes which lie in the x'-y' (aperture) plane, and whose centers are placed at $(x',y',z') = (-d/2,0,0)$ and $(d/2,0,0)$. The observation plane is defined by $z' = z$ for some positive constant z. This plane includes the x-axis, which is parallel to the x'-axis and is used in Eq. (1). The pattern of ellipses represents an intensity pattern generated on the observation plane by passing light through the two pinholes [1].

the power spectral density at the position of the pinholes. We note that the power spectral density that would be present along the x-axis with one pinhole closed is given by $S_1(x,\omega) \equiv |K_x(x)|^2|K_\omega(\omega)|^2 S_Q(\omega)$, and that the intensity along the x-axis with one pinhole closed is given by $I_0(x) = \int_{-\infty}^{\infty} S_1(x,\omega)\,\mathrm{d}\omega$. Then Eq. (1) can be rewritten in the following way:

$$I(x) = 2I_0(x)\left(1 + \mathrm{Re}\left[\int_{-\infty}^{\infty} s_1(\omega)\mu_\omega(\omega)\exp\left(-i\frac{\omega x d}{zc}\right)\mathrm{d}\omega\right]\right), \tag{2}$$

where $s_1(\omega) \equiv |K_\omega(\omega)|^2 S_Q(\omega)/\int_{-\infty}^{\infty}|K_\omega(\omega')|^2 S_Q(\omega')\,\mathrm{d}\omega' = S_1(x,\omega)/I_0(x)$ represents a normalized power spectral density along the x-axis, although it is apparently independent of x.

In actuality, the measurement of $I(x)$ by a real detector will be governed by the detector's spectral response function. Let $I'(x)$ be the *apparent* distribution sampled from $I(x)$ by the detector. In order to illuminate the difference between $I(x)$ and $I'(x)$ we note that a real detector will not measure $S_1(x,\omega)$ but rather $S_1(x,\omega)\eta(\omega)$ where $\eta(\omega)$ is the detector's spectral response function. Neglecting measurement noise, this leads to an explicit expression for the apparent intensity distribution:

$$\begin{aligned} I'(x) =& 2I_0'(x) + I_0'(x)\left[\int_{-\infty}^{\infty} s_{\eta\omega}(\omega)\mu_\omega(\omega)\exp\left(-i\frac{\omega x d}{zc}\right)\mathrm{d}\omega\right. \\ &\left. + \int_{-\infty}^{\infty} s_{\eta\omega}(\omega)\mu_\omega^*(\omega)\exp\left(i\frac{\omega x d}{zc}\right)\mathrm{d}\omega\right], \end{aligned} \tag{3}$$

where $s_{\eta\omega}(\omega) \equiv |K_\omega(\omega)|^2 S_Q(\omega)\eta(\omega)/\int_{-\infty}^{\infty}|K_\omega(\omega')|^2 S_Q(\omega')\eta(\omega')\,\mathrm{d}\omega'$ is the apparent, normalized power spectral density, and $I_0'(x) \equiv \int_{-\infty}^{\infty} S_1(x,\omega)\eta(\omega)\,\mathrm{d}\omega$ is the spatial intensity distribution that would be apparent to the detector from illuminating only one of the pinholes.

#204319 - $15.00 USD Received 10 Jan 2014; revised 20 Mar 2014; accepted 22 Mar 2014; published 1 Apr 2014

3.2. Transferring to the spatial frequency domain

We proceed in the spatial frequency domain with the goal of extracting functions of interest from $I'(x)$. Let $\tilde{I}'(f_x) \equiv \mathscr{F}\{I'(x)\}$, $\tilde{I}'_0(f_x) \equiv \mathscr{F}\{I'_0(x)\}$, $s_\eta(f_x) \equiv s_{\eta\omega}(2\pi z c f_x/d)$, and recall that $\mu_\omega(2\pi z c f_x/d) = \mu(f_x)$. Then the Fourier transform of Eq. (3) gives

$$\tilde{I}'(f_x) = 2\tilde{I}'_0(f_x) + \tilde{I}'_0(f_x) \otimes [s_\eta(-f_x)\mu(-f_x)] + \tilde{I}'_0(f_x) \otimes [s_\eta(f_x)\mu^*(f_x)], \tag{4}$$

where $\otimes$ indicates a convolution, $*$ indicates a complex conjugate, and we have used the fact that $s_\eta(f_x)$ represents a power spectral density and is therefore real and non-negative. We now define the following three functions, which arise as the three terms on the right hand side of Eq. (4):

$$\begin{aligned} A(f_x) &\equiv \tilde{I}'_0(f_x) \otimes [s_\eta(-f_x)\mu(-f_x)], \\ B(f_x) &\equiv 2\tilde{I}'_0(f_x), \text{ and} \\ C(f_x) &\equiv \tilde{I}'_0(f_x) \otimes [s_\eta(f_x)\mu^*(f_x)]. \end{aligned}$$

Note that $s_\eta(f_x)$ vanishes for $f_x < 0$ because it is defined in the analytic signal representation. The usefulness of working in the spatial frequency domain becomes clear when (a) the pinholes are small enough, which means $\tilde{I}'_0(f_x)$ is narrow enough, and (b) the non-zero portion of $s_\eta(f_x)$ is narrow enough such that Eq. (4) can be approximated as a sum of three non-overlapping functions [3, 26]:

$$\tilde{I}'(f_x) \approx \begin{cases} A(f_x) & : f_x < -c \\ B(f_x) & : -c \le f_x \le c \\ C(f_x) & : f_x > c \end{cases} \tag{5}$$

for some positive real constant c. Importantly, this means that given a plot of $\tilde{I}'(f_x)$ we can find each of A, B, and C by looking in their respective domains. The results which follow are obtained by approximating Eq. (5) in different ways.

3.3. The apparent, normalized power spectral density

First, we consider how $s_\eta(f_x)$ can be extracted by making two assumptions. We assume that the pinholes are very small such that we can make the approximation $\tilde{I}'_0(f_x) \approx \tilde{I}_1\delta(f_x)$, where $\tilde{I}_1 = \int_{-\infty}^{\infty} \tilde{I}'_0(f_x)\,\mathrm{d}f_x$ and $\delta(f_x)$ is the Dirac delta function. We further assume that the fields incident on the aperture have been prepared with a high degree of spatial coherence. This can be done, for example, by passing light from the source through a small aperture. It is important to note, however, that this or similar techniques may be inappropriate for use with fields whose statistical properties are shift-variant. This leads to the approximation $|\mu(f_x)| \approx |\mu_1|$, where μ_1 is a non-zero constant. These approximations give $|A(f_x)| \approx s_\eta(-f_x)|\tilde{I}_1\mu_1|$ and $|C(f_x)| \approx s_\eta(f_x)|\tilde{I}_1\mu_1^*|$. Under these approximations we can extract $s_\eta(f_x)$ through the relations

$$s_\eta(-f_x) \approx |A(f_x)| \Big/ \int_{-\infty}^{-c} |A(f_x)|\,\mathrm{d}f_x, \text{ and} \tag{6}$$

$$s_\eta(f_x) \approx |C(f_x)| \Big/ \int_{c}^{\infty} |C(f_x)|\,\mathrm{d}f_x. \tag{7}$$

3.4. The spectral degree of coherence

We consider now the case in which $s_\eta(f_x)$ is known by measurement but $\mu(f_x)$ is not constant. We proceed with the goal of extracting $\mu(f_x)$ from a measurement of $I'(x)$. We return to Eq. (5),

#204319 - $15.00 USD Received 10 Jan 2014; revised 20 Mar 2014; accepted 22 Mar 2014; published 1 Apr 2014

assuming $\tilde{I}_0'(f_x) \approx \tilde{I}_1 \delta(f_x)$, and find $A(f_x) \approx \tilde{I}_1 s_\eta(-f_x)\mu(-f_x)$, $B(f_x) \approx 2\tilde{I}_1 \delta(f_x)$, and $C(f_x) \approx \tilde{I}_1 s_\eta(f_x)\mu^*(f_x)$. Again, we can find each of A, B, and C by looking at a plot of $\tilde{I}'(f_x)$ in the corresponding domain. We can then extract $\mu(f_x)$, remembering that $s_\eta(f_x)$ is known in this case, by using either of the following relations:

$$\mu(-f_x) \approx \frac{2A(f_x)}{s_\eta(-f_x) \int_{-c}^{c} B(f_x)\,\mathrm{d}f_x}, \text{ and} \tag{8}$$

$$\mu^*(f_x) \approx \frac{2C(f_x)}{s_\eta(f_x) \int_{-c}^{c} B(f_x)\,\mathrm{d}f_x}. \tag{9}$$

It must be noted that these relations are only useful for extracting $\mu(f_x)$ at frequencies where $A(f_x)$, $B(f_x)$, $C(f_x)$, and $s_\eta(f_x)$ are measurable with sufficient signal-to-noise ratios.

Thus, by combining the results of Secs. 3.3 and 3.4, we have shown that by adding and then removing an aperture from a Thompson-Wolf experiment we can extract the spectral degree of coherence for the light at the position of the two pinhole aperture over a wavelength range within the response function of the detector. This is done without resorting to additional optical elements of any kind.

3.5. The spectral degree of coherence in relation to the complex degree of coherence

Separately, a measurement of the spectral degree of coherence can be made by using a series of optical filters in conjunction with the two-pinhole aperture. Given an optical filter with a sufficiently narrow passband, one can recover the spectral degree of coherence of the unfiltered light at the center passband wavelength from the equal time degree of coherence of the filtered light [27, 28]:

$$\mu_\omega(\omega_0) = \gamma^{(+)}(0), \tag{10}$$

where ω_0 is the center passband frequency and the $(+)$ indicates that the source has been spectrally filtered. Thus, the spectral degree of coherence can be measured by using a series of optical band-pass filters with different center wavelengths.

We proceed with the goal of extracting $\gamma^{(+)}(x)$ from $I^{(+)}(x)$. We note that, given a narrow passband, both $\eta(\omega)$ and $K_\omega(\omega)$, as defined in Sec. 3.1, can be considered as constant. Then, similar to Eq. (2), we have $I^{(+)}(x) = 2I_0^{(+)}(x)\left(1 + \mathrm{Re}\left[\int_{-\infty}^{\infty} s_\omega^{(+)}(\omega)\mu_\omega^{(+)}(\omega)\exp\left(-i\frac{\omega x d}{zc}\right)\mathrm{d}\omega\right]\right)$, except $s^{(+)}(f_x) \equiv s_\omega^{(+)}(\omega)$ now represents the normalized, spectrally filtered power spectral density *at the pinholes*. The Fourier transform of this equation gives

$$\tilde{I}^{(+)}(f_x) = 2\tilde{I}_0^{(+)}(f_x) \otimes \left(\delta(f_x) + \frac{1}{2}\left[s^{(+)}(-f_x)\mu^{(+)}(-f_x) + s^{(+)}(f_x)\mu^{(+)*}(f_x)\right]\right). \tag{11}$$

The spectral bandwidth condition (b) used in deriving Eq. (5) is somewhat relaxed because it is now fulfilled based on the width of the passband and not the width of the unfiltered spectrum. We define once again three functions: $A^{(+)}(f_x) \equiv \tilde{I}_0^{(+)}(f_x) \otimes \left[s^{(+)}(-f_x)\mu^{(+)}(-f_x)\right]$, $B^{(+)}(f_x) \equiv 2\tilde{I}_0^{(+)}(f_x)$, and $C^{(+)}(f_x) \equiv \tilde{I}_0^{(+)}(f_x) \otimes \left[s^{(+)}(f_x)\mu^{(+)*}(f_x)\right]$. Then, under small-pinhole and narrow-passband conditions, we have an equation similar to Eq. (5):

$$\tilde{I}^{(+)}(f_x) \approx \begin{cases} A^{(+)}(f_x) & : f_x < -c \\ B^{(+)}(f_x) & : -c \le f_x \le c \\ C^{(+)}(f_x) & : f_x > c. \end{cases} \tag{12}$$

#204319 - $15.00 USD Received 10 Jan 2014; revised 20 Mar 2014; accepted 22 Mar 2014; published 1 Apr 2014

The approximation that $\tilde{I}_0^{(+)}(f_x) \approx \tilde{I}_1^{(+)}\delta(f_x)$ is not necessary here. $\tilde{I}_0^{(+)}(f_x)$ and $s^{(+)}(f_x)$ need only be narrow enough such that $A^{(+)}(f_x)$, $B^{(+)}(f_x)$, and $C^{(+)}(f_x)$ do not overlap significantly. Then the three piecewise regions given in Eq. (12) can be separated by inspection.

It was shown by Friberg and Wolf [27] that the complex degree of coherence, $\gamma_\tau(\tau)$, is related to the spectral degree of coherence, $\mu_\omega(\omega)$, by a Fourier transform: $\gamma_\tau(\tau) = \mathscr{F}\{s_\omega(\omega)\mu_\omega(\omega)\}$, where $s_\omega(\omega)$ is the normalized power spectral density of the field at the pinholes. We now use the Fourier inverse to recover $\gamma^{(+)}(x)$:

$$\gamma^{(+)}(x) \approx \frac{\mathscr{F}^{-1}\left\{2A^{(+)}(f_x)\right\}}{\mathscr{F}^{-1}\left\{B^{(+)}(f_x)\right\}}, \text{ and} \tag{13}$$

$$\gamma^{(+)*}(x) \approx \frac{\mathscr{F}^{-1}\left\{2C^{(+)}(f_x)\right\}}{\mathscr{F}^{-1}\left\{B^{(+)}(f_x)\right\}}. \tag{14}$$

The function $\gamma^{(+)}(x)$ can be evaluated at $x = 0$ in order to find $\mu_\omega(\omega_0)$ using Eq. (10). It should be noted that Eqs. (13) and (14) will return noise at positions x where $\mathscr{F}^{-1}\{B^{(+)}(f_x)\}$ evaluates close to zero, but this will not be the case near $x = 0$.

We now return to Eq. (5) in order to recover $\gamma(x)$ in the unfiltered case. We define the following functions:

$$\gamma'(x) \equiv \frac{\mathscr{F}^{-1}\{2A(f_x)\}}{\mathscr{F}^{-1}\{B(f_x)\}}, \text{ and} \tag{15}$$

$$\gamma'^{*}(x) \equiv \frac{\mathscr{F}^{-1}\{2C(f_x)\}}{\mathscr{F}^{-1}\{B(f_x)\}}. \tag{16}$$

The recovery of $\gamma(x)$ from $\gamma'(x)$ is possible in cases where the spectral response function, $\eta(\omega)$, of the detector is known and is wider than the power spectral density at the pinholes, $S_Q(\omega)$, and the apparent, normalized power spectral density, $s_{\eta\omega}(\omega)$, is known by measurement. By Wolf [24], Eq. 3.1.3, we find that $|K_\omega(\omega)|^2 \propto \omega^2$. Let $\mathscr{W}$ be the set of all frequencies ω for which $\eta(\omega)$ is measurable with an acceptable signal-to-noise ratio. We define the following function:

$$\eta'(\omega) \equiv \begin{cases} \text{large} & : \omega \notin \mathscr{W} \\ \omega^2\eta(\omega) & : \omega \in \mathscr{W}. \end{cases}$$

In this case $\gamma(x)$ can recovered:

$$\gamma(x) \approx \mathscr{F}\left\{\frac{\mathscr{F}^{-1}\{\gamma'(x)\}}{\eta'(2\pi z c f_x/d)\int_0^\infty \frac{s_{\eta\omega}(\omega)}{\eta'(\omega)}\,\mathrm{d}\omega}\right\}, \tag{17}$$

where the reason for defining $\eta'(\omega)$ becomes clear from its position in the denominator. It has thus been shown that, under certain circumstances, both the spectral and complex degrees of coherence for light at the position of the two pinhole aperture in a Thompson-Wolf experiment can be extracted from the apparent interference pattern generated by such an aperture.

4. Experimental details, results, and discussion

A source with a known intensity distribution was used to test the efficacy of the apparatus. Light from a halogen lamp was passed through an optical fiber bundle. Coherence properties of the

#204319 - $15.00 USD Received 10 Jan 2014; revised 20 Mar 2014; accepted 22 Mar 2014; published 1 Apr 2014

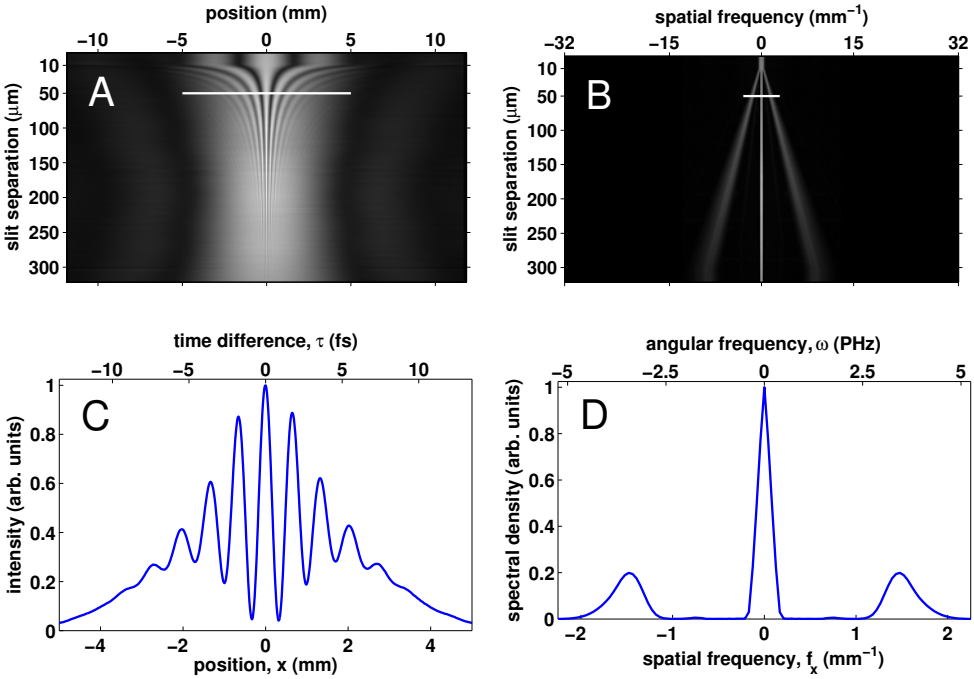

Fig. 4. (a) The intensity interferogram recorded by the apparatus at a distance of 4.5 m from the fiber bundle and (b) the associated amplitude spectral density given by a Fourier transform across the horizontal dimension. Each horizontal cross-section of the interferogram represents a Thompson-Wolf experiment with a different pinhole separation. The white lines in (a) and (b) correspond to the cross-sections given in (c) and (d), respectively, for a slit separation of 50 μm. The images shown in (a) and (b) have been scaled non-linearly to enhance contrast.

light emitted from the bundle were measured by the two-slit apparatus and compared to those expected by the van Cittert-Zernike theorem [24] as applied to an image of the fiber bundle end.

The two-slit aperture was placed at a distance of 4.5 m from the fiber bundle end. An iris, closed to a diameter of 2 mm, was placed directly in front of the bundle and a series of interferograms were recorded and averaged. The use of an iris to increase spatial coherence can be inappropriate if the normalized power spectral density varies across the surface of the source. In that case passing the light through an optical fiber or integrating sphere or placing the aperture far enough from the source may be more appropriate. At this distance, and with the reduced source size, the approximations necessary for the use of Eq. (6) are valid and the apparent power spectral density, $s_\eta(-f_x)$, was thereby extracted. A set of data associated with this measurement is shown in Fig. 4 and serves as an example for other measurements.

As shown in Fig. 4(a), and as expected from the relationship between x and τ, diffraction from the non-parallel double slit aperture produces interference fringes whose separation depends hyperbolically on the slit separation. Importantly, the slow variation in slit separation produces an interferogram in which negligible diffraction occurs across the vertical dimension. This allows for each horizontal cross-section of the interferogram to be used in approximating the result that would be obtained in a Thompson-Wolf experiment by a pinhole pair of the same separation distance. The Fourier transform associated with each horizontal cross-section can be found by transforming the entire image across the horizontal dimension, as shown in Fig. 4(b).

#204319 - $15.00 USD Received 10 Jan 2014; revised 20 Mar 2014; accepted 22 Mar 2014; published 1 Apr 2014

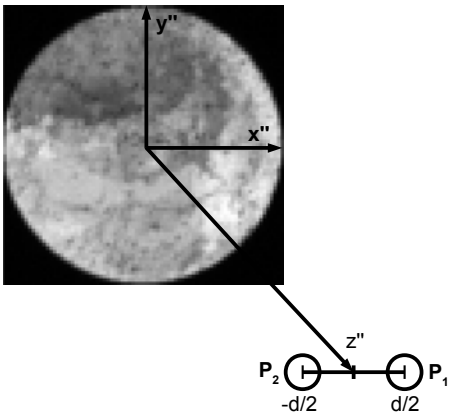

Fig. 5. The intensity distribution of light with 510 nm wavelength at the position of the fiber bundle source as measured by a camera. The diameter of the circular area is 0.62 cm. The shown coordinate axes were used in applying the van Cittert-Zernike theorem. The two circles represent the two pinholes at positions P_1 and P_2 of a Thompson-Wolf experiment where d is the center-to-center pinhole separation distance.

Thus, the equations given in Sec. 3 can be applied individually to each horizontal cross-section in order to extract the degree of coherence as a function of the slit separation distance.

An example set of cross-sectional data is shown in Figs. 4(c) and 4(d) for a slit separation of 50 μm. The broadband nature of the source is visible in Fig. 4(c) as a decrease in fringe visibility with distance from the center. This is seen more easily in Fig. 4(d), where the bands to the left and right of the central band correspond to a significant power spectral density across the optical frequency range. These bands also to correspond the functions $A(f_x)$, $B(f_x)$, and $C(f_x)$ as defined in Sec. 3.2. The spatially coherent nature of the source can be seen in the fact that the fringe visibility is good near $x = 0$ in Fig. 4(c) and from the fact that the combined area under the left and right bands of Fig. 4(d) is similar in magnitude to the area under the central band.

Next, the two-slit aperture was placed at an arbitrarily chosen distance of 105 cm from the fiber bundle end. It must be noted that the source-to-aperture distance affects the coherence properties of the light at the position of the slits and different results would have been found for other distances. Two more sets of interferograms were recorded and averaged, one set with an optical filter in place over the source, centered at 510 nm with a passband width of 10 nm, and one set without a filter. Optical effects related to the geometry of the apparatus were mitigated by post-processing as discussed in Appendix A. Equation (8) was used to extract the spectral degree of coherence, $\mu_\omega(\omega)$, from the unfiltered images in the wavelength regions to which the detector was sensitive (390-710 nm). Equations (10) and (13) were used to extract the spectral degree of coherence at 510 nm, $\mu(\lambda = 510\,\text{nm})$, from the filtered images.

In order to calculate the equal time degree of coherence expected by the van Cittert-Zernike theorem, the intensity distribution at the fiber output was measured with a camera and is shown in Fig. 5. The distribution was measured through an optical filter centered at 510 nm. It is assumed that the distribution pattern is constant in wavelength. A hyperspectral image would have been required for less well-behaved sources. The equal time degree of coherence between two points can be calculated for an incoherent source with a given quasi-monochromatic intensity distribution. Following Eqs. 3.2.11 and 3.2.12 from Wolf [24], we have the van Cittert-Zernike

#204319 - $15.00 USD Received 10 Jan 2014; revised 20 Mar 2014; accepted 22 Mar 2014; published 1 Apr 2014

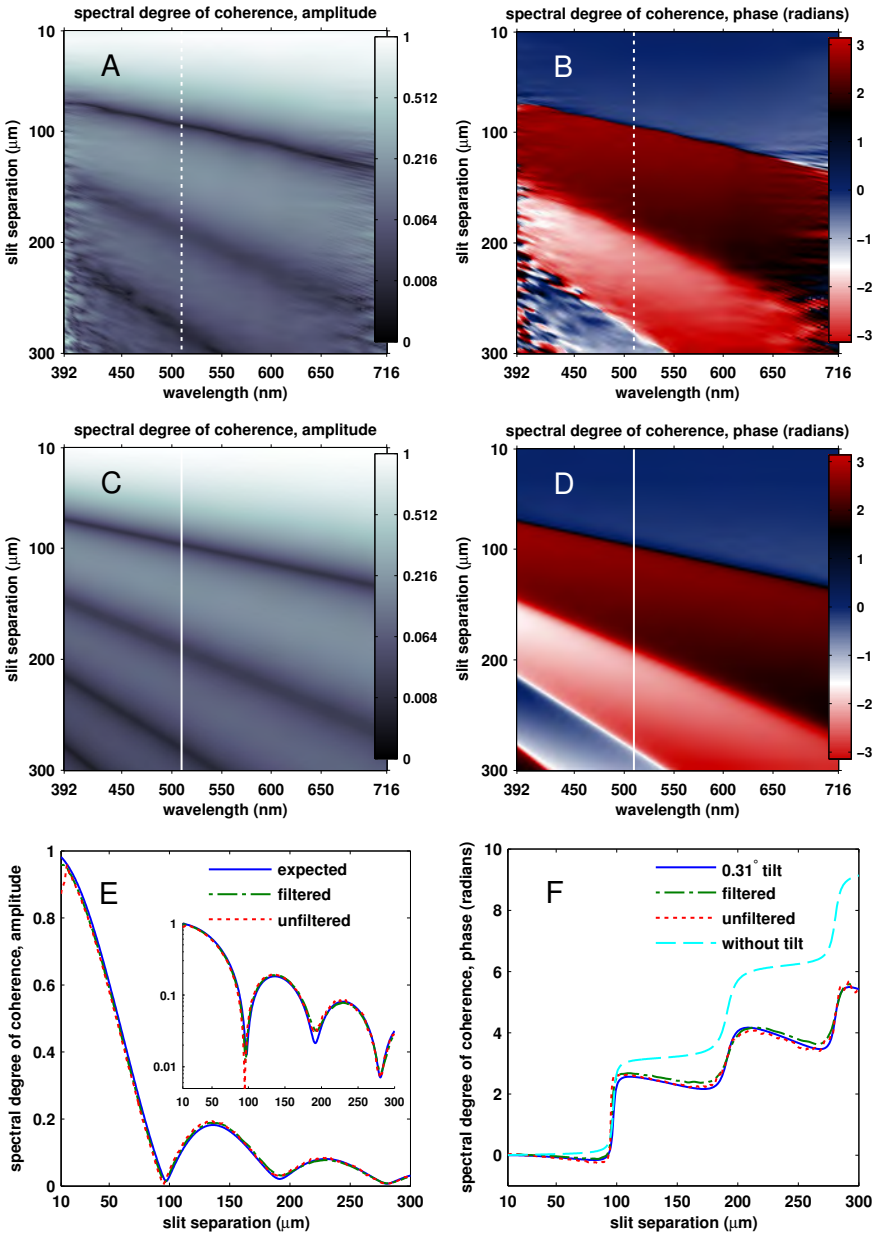

Fig. 6. Measured and expected spectral degree of coherence for light at a distance of 105 cm from the source shown in Fig. 5. (a) Amplitude and (b) phase of the spectral degree of coherence measured by the two-slit apparatus in the unfiltered case. (c) Amplitude and (d) phase of the spectral degree of coherence expected from the source by the van Cittert-Zernike theorem assuming that the intensity distribution is invariant in wavelength and a 0.31° aperture tilt relative to the detector. (e) Amplitude on linear and logarithmic (inset) scales and (f) unwrapped phase comparison between the filtered, unfiltered, and expected measurements at 510 nm wavelength. The phase comparison (f) includes the fit which incorporates the 0.31° tilt as described in the text as well as that expected without tilt. The vertical lines shown in each of (a-d) correspond to cross sections shown in the respective lines plotted in (e) and (f).

#204319 - $15.00 USD Received 10 Jan 2014; revised 20 Mar 2014; accepted 22 Mar 2014; published 1 Apr 2014

theorem:

$$j(P_1,P_2) = \frac{1}{\sqrt{I(P_1)}\sqrt{I(P_2)}} \int_\sigma I(S) \frac{e^{ik(R_2-R_1)}}{R_1 R_2} \mathrm{d}S, \text{ where} \tag{18}$$

$$I(P_n) = \int_\sigma \frac{I(S)}{R_n^2} \mathrm{d}S \ \ (n = 1,2). \tag{19}$$

Here, $j(P_1,P_2) \equiv \gamma_\tau(P_1,P_2,\tau = 0)$ is the equal time degree of coherence between points P_1 and P_2, $I(S)$ is the intensity distribution as a function of position S on the source σ, and $k = \omega/c$ is the wavenumber of the light. In the set of coordinates defined by Fig. 5, P_1 is at position $(x'',y'',z'') = (d/2,0,z)$ and P_2 is at position $(x'',y'',z'') = (-d/2,0,z)$ for some positive constant z, where z is much larger than the linear dimensions of the source. This gives $R_1 = ([x'' - \frac{d}{2}]^2 + y''^2 + z^2)^{1/2}$ and $R_2 = ([x'' + \frac{d}{2}]^2 + y''^2 + z^2)^{1/2}$ where x'' and y'' become the variables of integration in Eqs. (18) and (19). In this instance, for a fixed z, $j(P_1,P_2)$ becomes a function of only d and ω. As a consequence of Eq. (10), the spectral degree of coherence, $\mu_\omega(d,\omega)$, can be obtained directly from $j(d,\omega)$. Thus, the two-dimensional spectral degree of coherence function expected to be measured by an ensemble of Thompson-Wolf experiments can be calculated for this particular source.

Figure 6 gives the spectral degree of coherence function measured by the two-slit apparatus and is compared to that expected by the van Cittert-Zernike theorem as applied to the camera image of the source. The amplitude and phase measured by the apparatus with unfiltered light, given by Figs. 6(a) and 6(b), agree well with the expected function, given by Figs. 6(c) and 6(d). Figures 6(e) and 6(f) compare the amplitude and phase measured in the unfiltered and filtered cases against the expectation at 510 nm. The amplitude in both cases fits well across the entire range of slit separations apart from a deviation below 15 μm. The deviation is somewhat worse in the unfiltered case and is due to the fact that the approximations necessary to derive Eq. (8) begin to break down for small separations while those necessary to derive Eq. (13) remain more valid.

The phase, shown in Fig. 6(f), is much more sensitive to misalignment of the pinholes relative to the z''-axis (as defined in Fig. 5) than the amplitude. In this case, a fit was made by considering a sheared set of pinhole pairs which are displaced from center on the x''-axis with displacements that depend linearly on the slit separation. This shear is equivalent to a small tilt of the two-slit aperture relative to the detector. The shown fit was found by introducing the equivalent of a 0.31° aperture tilt. This tilt is within the alignment error of the apparatus. Further, this suggests a precise method with which to measure the relative tilt between such a two-slit aperture and detector in future studies. The expected amplitude, shown in Fig. 6(e), is relatively insensitive to this type of tilt misalignment.

5. Apparatus capabilities and limitations

The apparatus described in this paper offers several notable capabilities. First, both the complex and spectral degrees of coherence of light from a broadband source can be measured in two dimensions by recording only two images. If the power spectrum of the light and spectral response function of the detector are known *a priori* then only a single image need be recorded. This is in contrast to methods which require adjustable double slits or a monochromator, and therefore a large set of non-simultaneous measurements [3, 7], or methods which are suited to narrow-band sources [12]. This capability allows for the rapid measurement of a coherence function and could possibly be used with moving or transient sources. Next, the compact nature of the apparatus allows for extreme portability. This portability may be interesting for applications in calibration or certification of sources which require certain coherence properties. Most

#204319 - $15.00 USD Received 10 Jan 2014; revised 20 Mar 2014; accepted 22 Mar 2014; published 1 Apr 2014

importantly, this type of apparatus is appropriate for use with partially coherent sources where the van Cittert-Zernike theorem fails.

Along with these capabilities there are limitations which merit discussion. The primary limitation, namely the assumption made in deriving Eq. (1) that the power spectral density on each pinhole is identical, limits the use of the apparatus to fields whose statistical properties are locally-shift-invariant. The spatial extent of the two-slit aperture and the spectral density measurement method impart similar restrictions. As a result, the apparatus is best suited for use with fields that can be locally approximated under the Schell-model.

Second, the apparatus is limited by the length and variation of the slits. The slow variation in slit separation serves to minimize diffraction along the long dimension of the aperture but it still exists and is not treated here. Additionally, the linear variation in slit separation is simple to design and fabricate but leads to hyperbolic fringes. Along with diffraction, this leads to mixing of data at small slit separations for fields with some appreciable angular and spectral bandwidth. This mixing could be reduced by using slits where the separation varies hyperbolically such that the slits are more parallel for small slit separations.

6. Conclusion

We have shown that a double slit aperture, in which the slit separation slowly varies, can be used to rapidly measure the spectral degree of coherence function of light at the position of the slits. The aperture works by performing the equivalent of many simultaneous Thompson-Wolf experiments over a range of slit separations and wavelengths. By using a detector with a sufficiently wide spectral response, the same aperture can also be used to measure the complex degree of coherence of the light. An aperture of this type was used to measure the spectral degree of coherence function for light emitted by an incoherent, thermal source. The results of this measurement were compared to those expected by the van Cittert-Zernike theorem and found to agree in both amplitude and phase. This type of aperture is also appropriate for use with sources of various states of coherence where the van Cittert-Zernike theorem fails to be valid.

Appendix A: Mitigation of geometrical optical effects

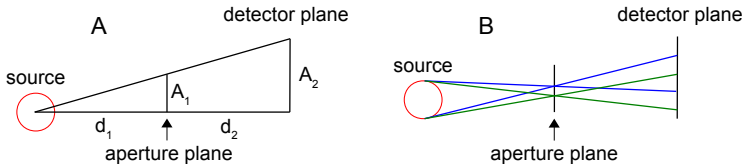

Fig. 7. Effects of geometry on the interferogram produced by a double slit. (a) A schematic of the geometrical magnification effect associated with light from any single position on the source which causes the illuminated spot produced on the detector to be larger than the aperture. The distances d_1, and d_2 are used in Eq. (20) to determine the magnification factor. (b) A schematic of the blurring effect associated with a finite-sized source. Light passing through one position on the slit can overlap on the detector with light passing through another position on the slit.

There are two prominent effects of geometry in the recorded interferogram images. The first is akin to pinhole camera magnification and the second is a blurring effect. Both effects stem from the fact that the detector was situated at a finite distance from the two-slit aperture and that the source had a finite size. These effects are illustrated in Fig. 7. The magnification effect

#204319 - $15.00 USD Received 10 Jan 2014; revised 20 Mar 2014; accepted 22 Mar 2014; published 1 Apr 2014

was removed by de-magnifying the images, through bi-linear interpolation of the data, across the long dimension of the aperture according to the following equation:

$$M = \frac{A_2}{A_1} = \frac{d_1 + d_2}{d_1}, \tag{20}$$

where M is the magnification and A_1, A_2, d_1, and d_2 are as described in Fig. 7. During the experiments considered here, both d_1 and d_2 were known by measurement. In general, d_1 may be unknown. In that case, a measurement of d_1 may be attempted based on measured and expected quasi-monochromatic fringe separations within the interferogram itself, but this could lead to larger systematic error than if d_1 were known. Otherwise, d_1 may be large enough such that the magnification can be neglected.

The blurring effect was mitigated by performing a deconvolution and a subsequent convolution. Since the spectrum and spectral degree of coherence data were measured with different source-to-aperture distances, the blurring effect was different in both cases. In principle, the blurring effect could be removed by a deconvolution with a certain unknown point spread function but this was not done. Instead, the blurring of both measurements was made the same. This was accomplished by first deconvolving a certain cross-section of the spectrum data, given in the spatial frequency domain and shown in Fig. 8(b), from the corresponding cross-section of spectral coherence data, shown in Fig. 8(a). A Lucy-Richardson deconvolution routine was used with a large number of iterations in order to find the point spread function that would lead to the spectral coherence cross-section from the spectrum cross-section via convolution. The entire spectrum image was then convolved along the vertical dimension with the recovered point spread function. This led to the same blur in both images.

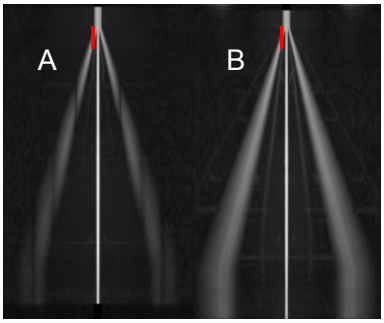

Fig. 8. The cross-sections which were used in the blurring mitigation method. The red line segments in both (a) the spectral degree of coherence data and (b) the spectrum data correspond to the positions of the considered cross-sections in the spatial frequency domain.

Acknowledgments

We thank P. Bharadwaj and M. Kasperczyk for fruitful discussions, M. Parzefall for creating Fig. 1 of this paper, and S. Riedi for assistance in fabricating the two-slit aperture. This project is funded by the Swiss National Science Foundation (SNF) under grant 200021_149433.